https://doi.org/10.7735/ksmte.2023.32.4.206

J. Korean Soc. Manuf. Technol. Eng.
ISSN 2508-5107(Online)

Check for updates

Droplet Mass and Length in a Piezoelectric Needle-valve Jetting Dispenser for a Power-law Fluid

Da-Hoon Park[a], Kwang Kim[a,*]

[a] Department of Mechanical Design Engineering, Tech University of Korea

ARTICLE INFO

Article history:
Received 30 Jun 2023
Revised 27 July 2023
Accepted 28 July 2023

Keywords:
Piezoelectric jet dispenser
Shear thinning
Droplet characteristics
CFD simulation

ABSTRACT

Jetting mass and droplet morphology variations in a high-viscosity power-law fluid dispensing system were investigated. A specialized dispensing system, containing a piezoelectric actuator, displacement amplifier, and needle-valve nozzle, was developed for high-viscosity fluids. Hydrogels served as non-Newtonian fluids, and a power-law model was employed to analyze the viscosity up to a shear rate of 1,000 (1/s). The needle, driven by a trapezoidal signal, acted as a piston, and changes in the jetted droplet mass and length were measured by varying the needle displacement and frequency. The experimental results well-matched the predicted ones (error: 10%). The needle movement generated Couette–Poiseuille flow, which increased the fluid shear rate and induced shear-thinning, in the dispensing chamber, thereby reducing the viscosity. A large number of droplets with similar masses (within 5%) and lengths were obtained at high driving stokes and frequencies. This analytical model is suitable for designing precise droplet-dispensing systems.

1. Introduction

Material jetting is utilized by dispensers[1,2] and three-dimensional (3D) printers[3,4], dispensing a small amount of material through a small diameter nozzle in droplets at room temperature, similar to inkjet printing. Drop-on-Demand (DOD) is a commercialized inkjet method, and fine droplets can be ejected according to the control method of the piezoelectric element.

In particular, this material jetting can be applied to fields requiring precision because they can inject an accurate amount of liquid. Additionally, the application of the jetting method reduces the stair-step effect[5] compared to the use of the fused deposition modeling (FDM) method, resulting in excellent surface quality[6]. The jetting methods include inkjet[7–9], binder jetting[10–12], and pneumatic jetting methods[13–15].

Low-viscosity inks, which are used in inkjet methods, are incompressible Newtonian fluids. Therefore, their viscosity does not change with pressure and speed. Various studies have been conducted on the accurate analysis of the volume and length of the ejected droplets. For example, Lu et al. experimentally studied the effects of the fluid and dispensing system parameters, such as pressure, viscosity, needle motion, and nozzle size, on droplet formation using computational fluid dynamics (CFD) software for a needle-valve type piezoelectric dispensing system[16,17]. Cheng et al. studied the effect of the

* Corresponding author. Tel.: +82-31-8041-0428
E-mail address: kimkwang@tukorea.ac.kr (Kwang Kim).

needle impact velocity on the droplet volume[18]. Antonopoulou et al. studied the effect of the surface tension and jetting velocity on the droplet length[19]. Studies based on Newtonian fluids with non-varying viscosities suggest a direction for the design and control of needle-valve type piezoelectric dispensing system.

The pneumatic jetting method involves jetting through a piezoelectric control valve, also known as a needle-valve-type piezoelectric dispenser. Compared to the use of the inkjet method, the jetting method can jet inks with a viscosity of several hundred Pa·s or higher, enabling the printing of materials with a high solid content, thereby resulting in reduced volume shrinkage and improved mechanical properties[20,21]. High-viscosity inks are typical non-Newtonian fluids that exhibit shear-thinning properties, and their viscosity changes with the pressure and velocity inside the ink chamber[22]. In particular, the viscosity of the fluid changes with an increase in the velocity of the fluid, resulting in an inaccurate analysis of the jetting flow rate and the shape of the jetting droplet compared to that of the inkjet method using low-viscosity fluids[23]. Therefore, experimental studies have been extensively conducted on needle-valve dispensing systems with non-Newtonian fluids. For non-Newtonian fluids, the effects of input signals and nozzle diameters on the formation and volume of droplets have been investigated[24,25]; however, the analysis of the formation and volume or mass of droplets is essential to fully reflect the viscosity change characteristics of non-Newtonian fluids due to needle movement.

This study aims to accurately predict the formation and mass of droplets in a needle-valve dispensing system with a non-Newtonian fluid by analyzing the characteristics of a non-Newtonian fluid whose viscosity changes with the movement of the needle. The shear rate of the non-Newtonian fluid due to the movement of the needle was characterized up to 1,000 (1/s), and the droplet formation and volume were calculated using the viscosity change test results in the fluid analysis. In addition, the shear-thinning characteristics were modeled by assuming a power law fluid to improve the accuracy of the analysis.

A needle-valve dispensing system was designed and built in-house to minimize analysis errors, and the needle drive was controlled using a trapezoidal signal. The movement of the needle was measured with a laser displacement meter. Moreover, the mass of the droplet was measured using an electronic balance, and a high-speed camera with a sufficient response to the driving frequency of the needle was used to analyze the droplet morphology. The mass and formation process of the droplets were analyzed by varying the stroke, driving displacement of the needle, and driving frequency.

The study results are expected to help in designing dispensers used in the semiconductor manufacturing and biofields, which require high-viscosity fluids to be dispensed in precise amounts.

2. Dispensing system design and analysis

2.1 Needle-valve piezoelectric jetting dispenser

Figure 1 illustrates the structure of a piezoelectric needle-valve system used to dispense high-viscosity fluids, such as adhesives or polymers, in small amounts. A needle-valve was used to control the opening and closing of the nozzle. The drive waveform of the piezoelectric actuator was applied using Labview, a DAQ (Data acquisition) board, and an internal sample clock. A laser displacement sensor (LK-G150, KEYENCE) with a resolution of 0.5 μm and a sampling period of 200 μs was used to measure the displacement of the needle, and the shape of the droplet from the nozzle was recorded with a high-speed camera (FASTCAM MINI UX50, Photron). The mass of the droplet was measured with an electronic balance (HR-200, A&D KOREA) with a resolution of 0.1 mg. When a voltage was applied to the piezoelectric actuator (P-844.60, PI GmbH & Co.), the piezoelectric material deformed and displaced the piston.

Figure 2(a) illustrates the piezoelectric needle-valve system. In particular, the displacement of the needle is amplified by the ratio of the areas $(Dpc_1/Dpc_2)^2$ of the top and bottom side of the piston chamber to approximately 365 μm in this study. The needle then moves up and down due to the deformation of the membrane. The movement increases the pressure inside the nozzle, which breaks the flow of the fluid through nozzle contact and releases the droplet due to the inertial force. The fluid is continuously pressurized for a constant flow throughout its path.

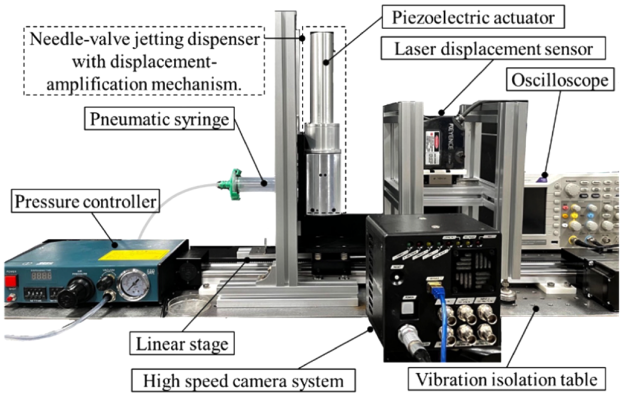

Fig. 1 An in-house design and built needle-valve dispensing system structure

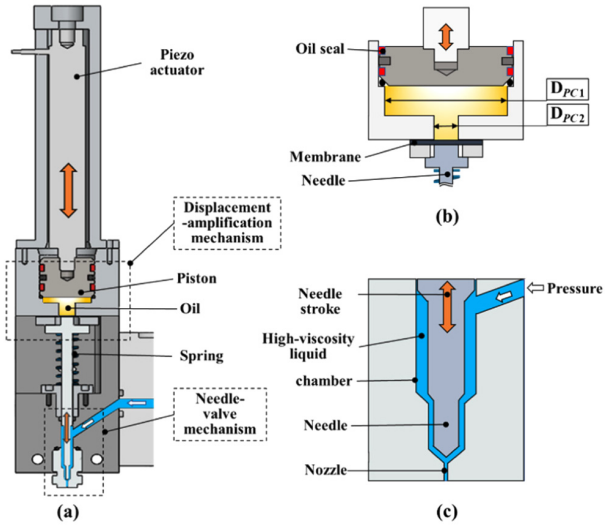

Fig. 2 Structure of the dispensing system: (a) piezoelectric needle-valve system; (b) displacement-amplification mechanism; (c) needle-valve

To force the fluid in the chamber out of the nozzle, it is necessary to pressurize it and secure the stroke of the needle. Thus, the chamber was pressurized to 4 bar with air, and the displacement of the needle was increased to 165 μm or higher. When the viscosity of the fluid is more than 1000 mPa·s, the displacement of the needle should be larger than 100 μm. In commercially available piezoelectric actuators, the displacement is approximately 50 μm at 100 V and 100 Hz, which is insufficient. Therefore, a displacement-amplification structure using different fluid cross sectional areas was designed, as illustrated in Figure 2(b). This structure is suitable as a displacement amplifier because of its rapid response characteristics in transmitting the motion of the piezoelectric actuator connected to the piston and the needle through incompressible oil. The shape and dimensions of the

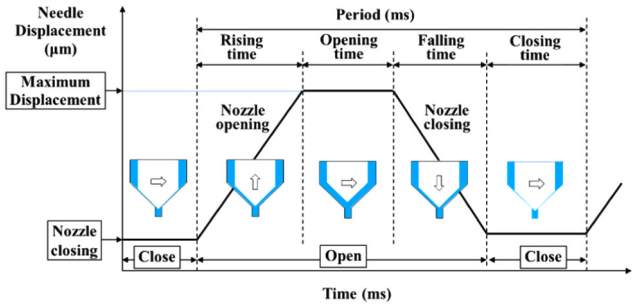

Fig. 3 Control signal for needle-valve movement

needle-valve part are illustrated in Figure 2(c). The up and down motion of the needle performs the function of a valve. In addition to the speed and displacement (stroke) of the needle, these parameters significantly impact the injection characteristics of the fluid.

The movement of the needle is controlled by applying a trapezoidal signal comprising four steps, as illustrated in Figure 3. Initially, the nozzle is closed by the needle, and during the rising time, the needle rises, and the nozzle opens. During the opening time, the needle moves up, opening the nozzle with a maximum displacement. Thereafter, during the falling time, the needle descends and gradually closes the nozzle. Finally, during the closing time, the needle closes the nozzle to stop the fluid from injection.

2.2 Needle-valve modeling for CFD analysis

The objective of this study is to understand the process of droplet formation and shape change using CFD analysis. Figure 4 illustrates the structure of a needle-valve system. To model the droplet injection using the piezoelectric dispenser device, we first defined the analysis regions as the outer region consisting of the bottom region of the chamber containing the fluid (L_{c1}, L_{c2}), needle region (L_n), and air (L_o). In the needle-valve type system, the part consisting of the needle, nozzle, and chamber is classified as the structure part and the fluid part in the chamber. The structure is classified as illustrated in Figures 4(a) and (b). After injection, the fluid exists in the air at the bottom side outside the nozzle.

The values of dimensional parameters for CFD are listed in Table 1. In the needle-valve type, the portion where the needle and the chamber are in contact is known as the seat. The seat angle of the part at which the top of the needle and the top of the chamber are in contact is denoted θ_2, and the angle at

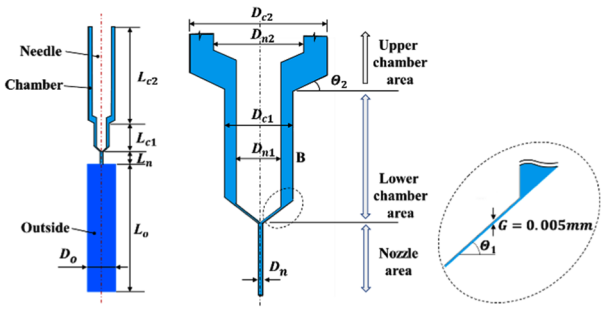

(a) Overall view (b) Detailed view (c) Closing gap

Fig. 4 Structure of the needle-valve system

Table 1 Dimensional parameters for CFD

Parameters	Value (mm)
Chamber diameter	(upper) D_{c2} = 6, (lower) D_{C1} = 3
Needle diameter	(upper) D_{n2} = 4, (lower) D_{n1} = 2
Chamber length	(upper) L_{c2} = 25, (lower) L_{c1} = 6
Nozzle diameter	Dn = 0.4
Nozzle length	Ln = 4
Outside diameter	Do = 7.0
Outside length	Lo = 80
Closed gap length	G = 0.005
Seat angle	θ_1 = 45°, θ_2 = 30°

Table 2 Properties of the fluid used in the simulation

	Air	Liquid
Density (kg/m^3)	1.225	990
Viscosity (mPa·s)	0.0179	Power law
Surface tension (N/m)	0.065	
Contact angle (°)	90	

which the needle and nozzle are in contact is θ_1. (Figure 4(c)). The computational domain must be continuous to perform CFD calculations. Therefore, the gap between the needle and valve must be set to zero. Moreover, the closing gap (G) was set to 0.005 mm to calculate the needle-valve ion system. A laminar flow model was applied to the flow in the chamber owing to the high fluid viscosity and a needle speed of less than 10 m/s. The surface of the high-viscosity fluid supplied to the top of the nozzle was set to follow the pressure inlet condition, assuming no pressure loss at the boundary.

The nozzle wall surface and the needle wall surface were set to the wall boundary condition, and the no slip condition was applied. Because the fluid area and flow change with time, the transient solver was applied. The characteristics of the fluid used in the analysis are listed in Table 2.

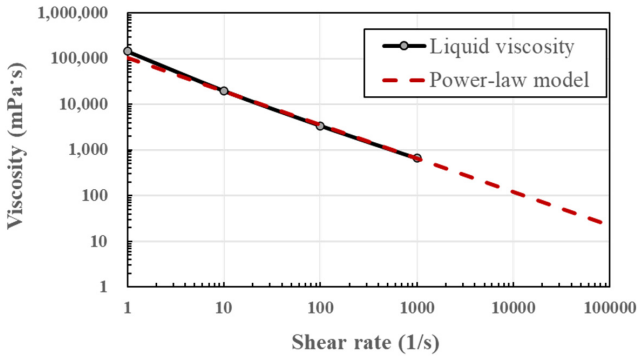

Fig. 5 Rheological properties of hydrogel

Table 3 Viscosity of the power-law liquid

Item	K (Pa·s^n)	n	μ_{max} (mPa·s)	μ_{min} (mPa·s)
Value	$10^{2.014}$	0.266	144,000	35

Table 4 Boundary condition used in the simulation

Fluid pressure (bar)	Operating frequency (Hz)	Needle displacement (μm)
4	40~120	165~365

In a needle-valve system, the rapid movement of the needle increases the shear rate of the fluid, which increases its fluidity and decreases its viscosity. The hydrogel (Sono Jelly, MEDITOP Corp.) used in this study corresponds to a non-Newtonian fluid with high-viscosity characteristics, and the fast movement of the needle causes a shear-thinning phenomenon that reduces its viscosity. To analyze the accurate dispensing of droplets, the rheological properties obtained through experiments where the shear rate of the hydrogel was extended to 1,000 (1/s) are illustrated in Figure 5, and CFD analysis was performed by applying the power law model, as shown in Eq. (1).

$$\mu = K\dot{\gamma}^{n-1}(\mu_{min} \le \mu \le \mu_{max}) \quad (1)$$

where n is the behavior index; K is the consistency index (power law index); $\dot{\gamma}$ is the shear rate; and μ_{min} and μ_{max} are the maximum and minimum viscosities used in the CFD analysis, respectively. Table 3 lists the values of the power law model parameters.

2.3 Flow characteristics in the needle valve

The commercial software Fluent and a dynamic mesh were applied to understand the effects of the needle movement on the velocity and the relationship to the trapezoidal drive signal.

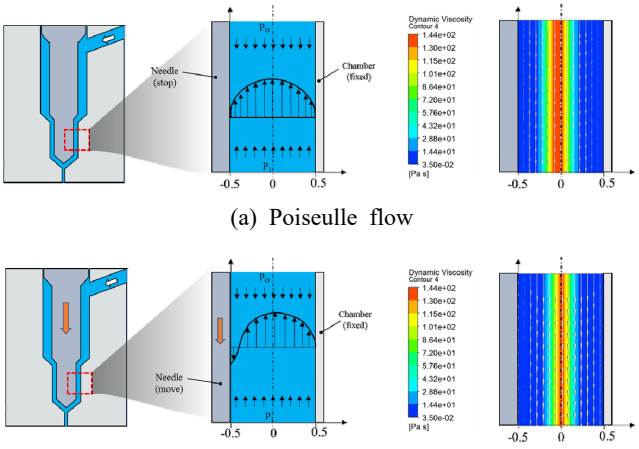

(a) Poiseuille flow

(b) Couette-Poiseuille flow

Fig. 6 Changes in the shear force and viscosity according to the needle movement

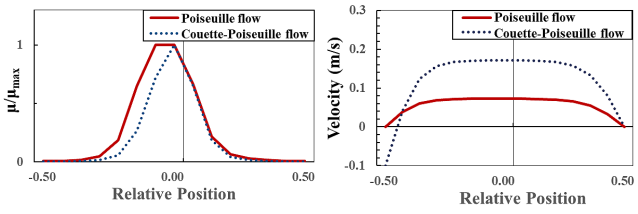

(a) Viscosity (b) Flow velocity

Fig. 7 Flow change in the chamber depending on the needle movement

The velocity distribution of the fluid in the stationary and moving states is illustrated in Figures 6(a) and (b), respectively. The objective of this study is to understand the process of droplet formation and shape change using CFD analysis. Poiseuille flow was applied when the needle was stationary. In contrast, when the needle was moving, the combined Poiseuille and Couette flows were applied. In the case of Poiseuille–Couette flow, the flow velocity between the chamber and the needle is more than two times higher than that in the case of the Poiseuille flow, depending on whether the needle is moving, as illustrated in Figure 7(a). The shear rate increases accordingly, and it decreases in the high-viscosity regime in the Poiseuille-Couette flow, as illustrated in Figure 7(b). Therefore, the flow rate increases when the needle is in motion compared to when the needle is stationary.

When a trapezoidal drive signal is applied to the needle, the fluid in the chamber is jetted, and droplets are formed, as illustrated in Figure 8, in both simulation and experiment.

In the initial state, the nozzle is closed by the needle and filled with fluid. In section ⓐ, the nozzle is opened because

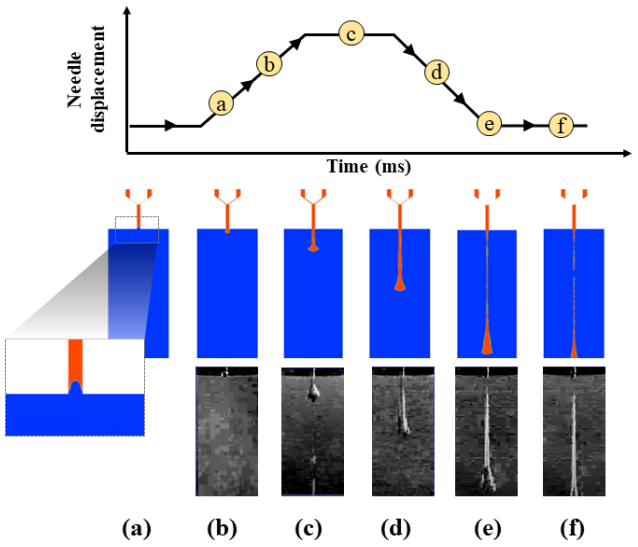

Fig. 8 Droplet morphologies in a jetting cycle (pressure: 4 bar; needle stroke: 165 μm; frequency: 120 Hz): (a) back flow; (b) growth; (c–d) extension; (e) breakage; (f) separation

of the rise of the needle, and a space is created above the nozzle. This creates an instantaneous negative pressure, causing the fluid at the inlet side of the nozzle to flow back toward the chamber, forming a concave surface owing to surface tension, as illustrated in Figure 8(a). In section ⓑ, where the needle continues to rise, the internal pressure acting on the fluid in the chamber creates a flow in the direction of the nozzle outlet, forming a convex shape, as illustrated in Figure 8(b). In section ⓒ–ⓓ, where the needle descends from the maximum displacement, the amount of injection from the nozzle increases owing to the shear-thinning phenomenon, where the viscosity decreases because of the increased shear rate due to the acceleration of the needle. Therefore, the initial droplet separates from the nozzle and forms a fluid filament, as illustrated in Figure 8(c)–(d). In section ⓔ, where the needle descends to the lowest point, the droplet has the largest size, as illustrated in Figure 8(e). As the needle contacts the nozzle, no more fluid is supplied into the nozzle. Thereafter, the droplet stretches its fluid filament owing to an inertial force. The fluid filament becomes thinner in section ⓕ where the nozzle is closed, and the droplet separates, as illustrated in Figure 8(f). The fluid filament part moves rapidly to the droplet because of surface tension; however, the droplet does not form a spherical shape owing to its high viscosity.

Subsequently, we analyzed the mass and shape changes of

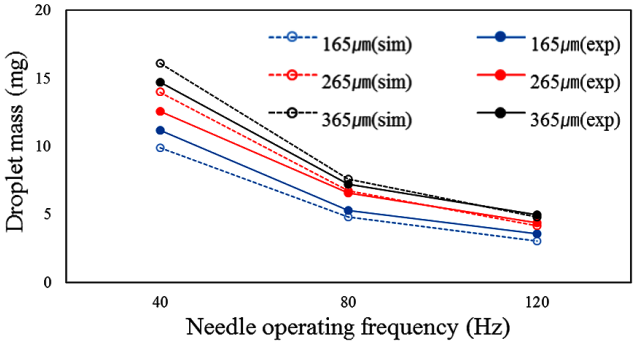

(a) Variation as a function of needle operating frequency

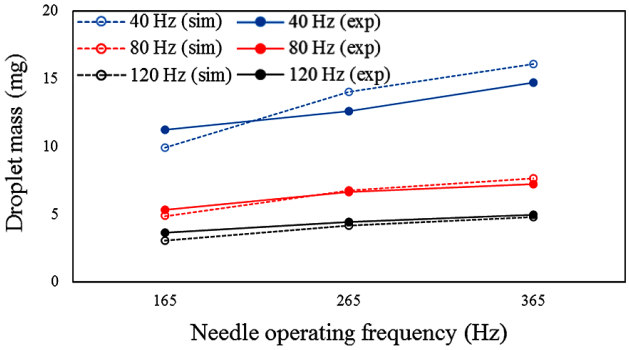

(b) Variation as a function of needle displacement

Fig. 9 The droplet mass at 4 bar as a function of needle operating frequency and needle displacement

the droplet. The internal pressure for overcoming the viscosity of the fluid and forming droplets was set to 4 bar. The kinetic displacement of the needle was increased by 100 μm from 165 μm to 265 and then to 365 μm, and the driving frequency was increased in intervals of 40 Hz from 40 to 120 Hz. Variation in the droplet mass with the driving frequency and needle displacement are illustrated in Figures 9(a) and (b), respectively. The mass of the droplets was obtained by dividing the total mass of the injected liquid by the number of droplets, and the average value after three experiments was used in calculations to reduce the measurement error. As shown in Figure 9(a), the mass of the droplet increases at low driving frequencies because the opening time of the nozzle is prolonged, increasing the flow rate.

At a given frequency, the mass of the droplet increases when the displacement of the needle is large because the needle moves through a large distance during a given interval. This increases the shear rate of the fluid with the needle velocity, increasing the flow rate owing to the viscosity-reducing, shear-thinning phenomenon. Figure 9(b) indicates that for a

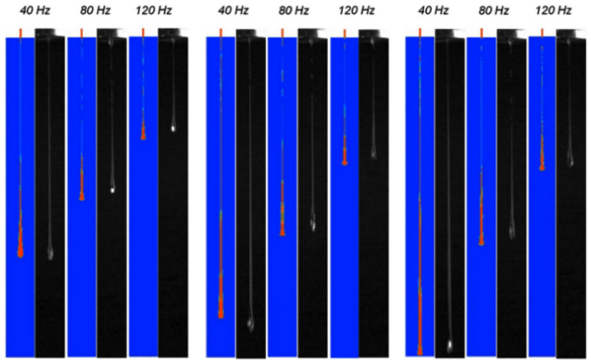

(a) 165 μm (b) 265 μm (c) 365 μm

Fig. 10 Jetting droplet formation shape depending on the needle stroke and driving frequency: Blue images show the CFD analysis results, and the black and white images show the experimental results

given needle displacement, the nozzle opening time increases at low frequencies. Therefore, the mass of the injected droplet changes with the driving frequency and stroke of the needle. Comparing the analysis findings with the experimental results, the error is within 10% at 265 and 365 μm, where the displacement of the needle is large; however, the error is more than 10% at 165 μm, with the lowest flow rate. In addition, at 80 Hz, the difference in the mass of the droplet with respect to the magnitude of the displacement is stable within 10%. Particularly, with a high driving frequency of 120 Hz and a large displacement of 365 μm, the difference between the calculated and measured value was 3.5%, demonstrating the reliability of the analysis. The aforementioned results suggest that at higher frequencies, such as 80 and 120 Hz, the CFD analysis predicts droplet mass with better accuracy.

In the hydrogel, which is a non-Newtonian fluid, the needle is stationary during the opening time, as shown in Figure 3, and the shear rate decreases, resulting in a change in the viscosity of the fluid. As the driving frequency increases, the opening time is shortened, and the change in viscosity is reduced, which is considered to reduce the error from the experiment.

The jetting shape of the droplet obtained by varying the driving frequency and displacement of the needle in the CFD analysis is shown in Figure 10 along with the photograph of the jetted droplet captured using a high-speed camera. The analytical and experimental results were compared in a section at a height of 80 mm. The blue images indicate the analytical results. Moreover, the black and white images are the results

captured using a high-speed camera. When the displacement of the needle is maintained constant, the droplet shortens with an increase in the driving frequency.

In contrast, it elongates with decreasing driving frequency owing to the long nozzle opening times. Furthermore, when the needle displacement increases while maintaining a constant frequency, the droplet elongates because the speed of the needle movement increases, reducing viscosity and pushing large fluid volumes toward the nozzle. As the driving frequency increases, the change in the droplet length is small, even with an increased needle displacement, because the nozzle opening time is short at high frequencies. For this needle-valve dispenser, the hydrogel was modeled as a power-law fluid to predict the change in viscosity with the shear rate owing to needle movement, and the results of the CFD analysis were in good agreement with the experimental values.

3. Conclusion

A power law model that fully reflects the shear rate up to 1,000 (1/s) in a non-Newtonian fluid was developed to perform fluid analysis and investigate the accurate jetting behavior of droplets in a droplet dispenser combining a piezoelectric element with a needle-valve method for jetting a precise amount of hydrogel, which is a high-viscosity fluid. An in-house built needle-valve jetting dispenser was modelled to minimize the error of the analysis, and the obtained results matched the experimental results within a 10% error. The following conclusions were obtained from this study.

A Couette–Poiseuille flow was generated when the needle was in motion. When the internal pressure was maintained at 4 bar, and the driving frequency and stroke of the needle were set to 120 Hz and 365 μm, respectively, the fluid flow velocity between the chamber and the needle increased by more than two times relative to that in the case of a stationary needle, and shear thinning occurred.

When the driving frequency of the needle was relatively high, the analytical results of the mass of the droplet were consistent with the experimental results within a 10% error. When the driving frequency was high at 120 Hz, and the stroke of the needle was large at 365 μm, the difference between the analysis and experimental results was 3.4%. This result highlights the high reliability of the analysis results.

The shapes and lengths of droplets obtained experimentally were similar to those obtained through the analysis. The opening time of the nozzle is the longest at 40 Hz. At a given needle displacement, the lower the driving frequency, the longer the droplet. At the same driving frequency, the larger the driving displacement of the needle, the longer the droplet. However, when the driving frequency is increased to 80 and 120 Hz, the increase in the length and mass of the droplet is decreased owing to shorter nozzle opening times at higher frequencies.

The results of the CFD analysis, obtained using a power series model considering the shear rate of non-Newtonian viscous fluids and reflecting the viscosity change, are consistent with the experimental values. Therefore, the mass and shape of the droplets can be accurately predicted using the CFD analysis, which can be helpful for dispensing system design in various fields such as semiconductor and bio industries.

To realize high-speed dispensing systems using high-viscosity fluids, the length of droplets must be further shortened in high-frequency driving. In future work, it should be investigated whether it is possible to shorten the length of the jetted droplet by optimizing the drive signal applied to the needle for each section.

Acknowledgement

This work was partially supported by the [GRRC program of Gyeonggi province] grant number [GRRC-KPU2020-B01], and [Korea Institute for Advancement of Technology (KIAT) grant funded by the Korea Government (MOTIE)] (P0008458; the HRD Program for Industrial Innovation).

References

[1] Nguyen, Q. H., Choi, M. K., Choi, S. B., 2008, A New Type of Piezostack-driven Jetting Dispenser for Semiconductor Electronic Packaging: Modeling and Control, Smart Mater. Struct., 17 015033, https://doi.org/10.1088/0964-1726/17/

01/015033.

[2] Wang, L., Du, J., Luo, Z., Du, X., Li, Y., Liu, J., Sun, D., 2012, Design and Experiment of a Jetting Dispenser Driven by Piezostack Actuator, IEEE Trans. Compon. Packag. Manuf. Technol., 3:1 147-156, https://doi.org/10.1109/TCPMT.2012.2222407.

[3] Jabari, E., Liravi, F., Davoodi, E., Lin, L., Toyserkani, E., 2020, High Speed 3D Material-jetting Additive Manufacturing of Viscous Graphene-based Ink with High Electrical Conductivity, Addit. Manuf., 35 101330, https://doi.org/10.1016/j.addma.2020.101330.

[4] Tyagi, S., Yadav, A., Deshmukh, S., 2022, Review on Mechanical Characterization of 3D Printed Parts Created using Material Jetting Process, Mater. Today: Proc., 51 1012-1016, https://doi.org/10.1016/j.matpr.2021.07.073.

[5] Singamneni, S., Roychoudhury, A., Diegel, O., Huang, B., 2012, Modeling and Evaluation of Curved Layer Fused Deposition, J. Mater. Process. Technol., 212:1 27-35, https://doi.org/10.1016/j.jmatprotec.2011.08.001.

[6] Gülcan, O., Günaydın, K., Tamer, A., 2021, The State of the Art of Material Jetting: A Critical Review, Polymers, 13:16 2829, https://doi.org/10.3390/polym13162829.

[7] Saleh, E., Zhang, F., He, Y., Vaithilingam, J., Fernandez, J. L., Wildman, R., Ashcroft, I., Hague, R., Dickens, P., Tuck, C., 2017, 3D Inkjet Printing of Electronics using UV Conversion, Adv. Mater. Technol., 2:10 1700134, https://doi.org/10.1002/admt.201700134.

[8] Kyobula, M., Adedeji, A., Alexander, M. R., Saleh, E., Wildman, R., Ashcroft, I., Gellert, P. R., Roberts, C. J., 2017, 3D Inkjet Printing of Tablets Exploiting Bespoke Complex Geometries for Controlled and Tunable Drug Release, J. Control. Release, 261 207–215, https://doi.org/10.1016/j.jconrel.2017.06.025.

[9] Negro, A., Cherbuin, T., Lutolf, M. P., 2018, 3D Inkjet Printing of Complex, Cell-laden Hydrogel Structures, Sci. Rep., 8 17099, https://doi.org/10.1038/s41598-018-35504-2.

[10] Mostafaei, A., Elliott, A. M., Barnes, J. E., Li, F., Tan, W., Cramer, C. L., Nandwana, P., Chmielus, M., 2021, Binder Jet 3D Printing: Process Parameters, Materials, Properties, Modeling, and Challenges, Prog. Mater. Sci., 119 100707, https://doi.org/10.1016/j.pmatsci.2020.100707.

[11] Gibson, I., Rosen, D., Stucker, B., Khorasani, M., 2021, Binder Jetting, In: Additive Manufacturing Technologies, Springer, Cham., 237-252, https://doi.org/10.1007/978-3-030-56127-7.

[12] Afshar-Mohajer, N., Wu, C. Y., Ladun, T., Rajon, D. A., Huang, Y., 2015, Characterization of Particulate Matters and Total VOC Emissions from a Binder Jetting 3D Printer, Build. Environ., 93:2 293-301, https://doi.org/10.1016/j.buildenv.2015.07.013.

[13] Yang, H., He, Y., Tuck, C., Wildman, R., Ashcroft, I., Dickens, P., Hague, R., 2013, High Viscosity Jetting System for 3D Reactive Inkjet Printing, International Solid Freeform Fabrication Symposium, University of Texas at Austin, 505-513, http://doi.org/10.26153/tsw/15576.

[14] Davoodi, E., Fayazfar, H., Liravi, F., Jabari, E., Toyserkani, E., 2020, Drop-on-demand High-speed 3D Printing of Flexible Milled Carbon Fiber/Silicone Composite Sensors for Wearable Biomonitoring Devices, Addit. Manuf., 32 101016, https://doi.org/10.1016/j.addma.2019.101016.

[15] Xiao, X., Li, G., Liu, T., Gu, M., 2022, Experimental Study of the Jetting Behavior of High-viscosity Nanosilver Inks in Inkjet-based 3D Printing, Nanomaterials, 12:17 3076, https://doi.org/10.3390/nano12173076.

[16] Lu, S., Zhou, F., Liu, W., Ren, C., Yan, F., 2017, Research of Biological Reagent Droplet Formation in Valve-control Dispensing Method, 7th IEEE International Conference on Electronics Information and Emergency Communication (ICEIEC), 473-476, https://doi.org/10.1109/ICEIEC.2017.8076608.

[17] Lu, S., Cao, G., Zheng, H., Li, D., Shi, M., Qi, J., 2018, Simulation and Experiment on Droplet Formation and Separation for Needle-type Micro-liquid Jetting Dispenser, Micromachines, 9:7 330, https://doi.org/10.3390/mi9070330.

[18] Cheng, X., Deng, G., Zhou, C., Wang, N., Cui, W., 2017, Study on the Process of Fluid jet Dispensing based on High and Low Voltage Drive, 18th International Conference on Electronic Packaging Technology (ICEPT), 262-265, https://doi.org/10.1109/ICEPT.2017.8046451.

[19] Antonopoulou, E., Harlen, O. G., Walkley, M. A., Kapur, N., 2020, Jetting Behavior in Drop-on-demand Printing: Laboratory Experiments and Numerical Simulations, Phys. Rev. Fluids, 5:4 043603, https://doi.org/10.1103/PhysRevFluids.5.043603.

[20] Ledesma-Fernandez, J., Tuck, C., Hague, R., 2014, High Viscosity Jetting of Conductive and Dielectric Pastes for Printed Electronics, 2014 International Solid Freeform Fabrication

Symposium, 4-6.
[21] Brent Strong, A., Hauwiller, P. B., 1989, Incremental Forming of Large Thermoplastic Composites, J. Thermoplast., 2:2 122-132, https://doi.org/10.1177/089270578900200204.
[22] Hoath, S. D., Castrejen-Pita, J. R., Hsiao, W. K., Jung, S., Martin, G. D., Hutchings, I. M., Tuladhar, T. R., Vadillo, D. C., Butler, S. A., Mackley, M. R., McIlroy, C., Morrison, N. F., Harlen, O. G., Yow, H. N., 2013, Jetting of Complex Fluids, J. Imag. Sci. Technol., 57:4 40403-1, https://doi.org/10.2352/J.ImagingSci.Technol.2013.57.4.040403.
[23] Vadodaria, S., Mills, T., 2020, Jetting-based 3D Printing of Edible Materials, Food Hydrocoll., 106 105857, https://doi.org/10.1016/j.foodhyd.2020.105857.
[24] Sun, C., Chu, X., Chen, J., Chen, D., Ren, J., Yuan, S., 2022, The Jetting Process and Spreading Characteristics of the Power-law Fluids for Material Jetting Process, Smart Mater. Struct., 31 115029, https://doi.org/10.1088/1361-665X/ac9bad.
[25] Zhou, C., Deng, G., Li, J., Duan, J. A., 2018, Flow Channel Influence of a Collision-based Piezoelectric Jetting Dispenser on Jet Performance, Sensors, 18:4 1270, https://doi.org/10.3390/s18041270.

Da-Hoon Park
M.S. in the Department of Mechanical Design Engineering, Tech University of Korea. His research interests are 3D Printer Technology Including Piezo Actuator Control and Engineering Aimulation.
E-mail: ekgns123123@tukorea.ac.kr

Kwang Kim
Professor in the Department of Mechanical Design Engineering, Tech University of Korea. His research interests are 3D Printer and Hydraulic Attachments Design, and Food Waste Drying Technology.
E-mail: kimkwang@tukorea.ac.kr